

# Isomeric Structural Characterization of Polyhedral Oligomeric Silsesquioxanes (POSS) with Styryl and Epoxy Phenyl Capping Agents

Erin Shammel Baker,<sup>†</sup> Jennifer Gidden,<sup>†</sup> Stanley E. Anderson,<sup>‡</sup>  
Timothy S. Haddad,<sup>§</sup> and Michael T. Bowers<sup>\*,†</sup>

Department of Chemistry & Biochemistry, University of California,  
Santa Barbara, California 93106, Department of Chemistry, Westmont College,  
Santa Barbara, California 93108, and ERC Inc., Air Force Research Laboratory,  
10 East Saturn Boulevard, Building 8451, Edwards AFB, California 93524-7680

Received January 7, 2004; Revised Manuscript Received March 1, 2004

## ABSTRACT

Ion mobility and molecular modeling methods were used to examine the gas-phase structures of sodiated POSS capped with styryl and epoxy phenyl substituents ( $\text{Na}^+\text{Sty}_x\text{Ep}_{8-x}\text{T}_8$ ). Results were obtained for  $x = 5-7$  and indicated that three distinct isomers with different collision cross-sections were present for each value of  $x$ . Theoretical modeling also yielded three different families of structures for each POSS system, and their calculated cross-sections agreed very well with experimental values (<1% difference). For  $\text{Na}^+\text{Sty}_7\text{EpT}_8$ , the three families differ in the number of "paired" Sty groups. For  $\text{Na}^+\text{Sty}_6\text{Ep}_2\text{T}_8$  and  $\text{Na}^+\text{Sty}_5\text{Ep}_3\text{T}_8$ , the three isomers correspond to the three different ways the Ep groups can be positioned on the POSS cage.

Inorganic–organic materials research is a rich and fast-developing area of nanotechnology that promises to provide a wide variety of commercial applications. Nanocomposites, derived from distinctly dissimilar inorganic and organic subunits combined on a nanometer length scale, can have extraordinary properties. Their macroscopic properties are usually superior to those found for conventional microscale composites due to the morphology and interfacial characteristics derived from mixing dissimilar materials on such tiny length scales. By adding inorganic components into organic polymers, mechanical,<sup>1</sup> thermal,<sup>2–5</sup> electrical,<sup>6</sup> and magnetic<sup>7</sup> properties are altered from those of pure organic polymers. These property advances have caused a surge of interest in nanocomposite synthesis and analysis with the promise of new applications in many fields, including nonlinear optics, sensors, and nanowires.<sup>8,9</sup>

Polyhedral oligomeric silsesquioxanes (POSS) are one type of material capable of forming nanocomposites.<sup>10,11</sup> POSS cages are nanoscopic in size and composed of a rigid three-dimensional Si–O framework of the form  $(\text{RSiO}_{3/2})_n$ , where R is typically an alkyl or aryl organic group. The properties of POSS are unique since one or more of the organic groups

can be made reactive for polymerization, while the remaining unreactive groups solubilize the inorganic core and allow for control over the interfacial interactions occurring between POSS and the polymer matrix.<sup>12–14</sup> POSS units can be added to virtually all polymer types either by blending,<sup>15</sup> grafting,<sup>16–18</sup> or copolymerization reactions.<sup>19–24</sup> By incorporating the rigid Si–O cage into polymers, property enhancements such as increased thermal stability, reduced flammability, reduced viscosity, and lowered density have been observed.<sup>11–26</sup> These property enhancements make POSS compounds of great interest to further improve high performance polymers and to develop multifunctional materials.

To study different POSS conformers, a technique has been developed in our group to incorporate both mass spectrometry and ion mobility<sup>27–29</sup> into the analysis so ions can be studied based on their mass and conformational size. With the help of matrix assisted laser desorption/ionization (MALDI)<sup>30</sup> and time-of-flight (TOF) mass spectrometry, ions in a sample can be identified by their mass and their relative abundance can be determined. Ion mobility then allows the ion of interest to be mass-selected and analyzed as a function of time while it drifts through a buffer gas under the influence of a uniform, weak electric field. Structural analysis can be performed on the ion depending on the amount of time it takes the ion to drift through the buffer gas and arrive at the detector.

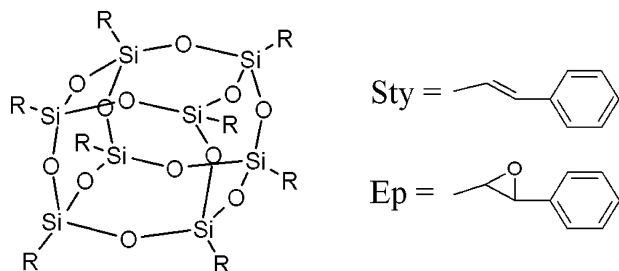
\* Corresponding author. E-mail: bowers@chem.ucsb.edu.

<sup>†</sup> University of California.

<sup>‡</sup> Westmont College.

<sup>§</sup> ERC Inc.

In this paper we report on the application of ion mobility to the structural analysis of POSS monomers cationized by sodium with a mixture of styryl (Sty) and epoxy phenyl (Ep) capping substituents ( $\text{Na}^+\text{Sty}_x\text{Ep}_{8-x}\text{T}_8$ ). The Ep group differs from the Sty capping substituent only by the epoxidation of the vinyl linkage, which connects the phenyl group to the Si–O cage.



Mixed  $\text{Sty}_x\text{Ep}_{8-x}\text{T}_8$  POSS systems were designed for incorporation into linear polymers and network resins.  $\text{Sty}_8\text{T}_8$  can be blended with various organic polymers, but with the epoxidation of the vinyl linkages, it is possible to cross-link the POSS into a cured epoxy network. The reactions of the Ep substituents with polyamines form amino alcohols that can further react with another Ep group to make a network cross-link.<sup>31,32</sup> Also, having both Sty and Ep groups on the exterior of the POSS cage has allowed for the polymerization of the mixed  $\text{Sty}_x\text{Ep}_{8-x}\text{T}_8$  POSS systems into vinyl ester, phenolic, epoxy, and dicyclopentadiene (DCPD) resins.<sup>33</sup> The ability to produce so many different resins has proved that having many functionalized substituents is essential in developing improved nanocomposites. Thus, to develop better nanocomposites, it is essential to fully understand how the  $\text{Sty}_x\text{Ep}_{8-x}\text{T}_8$  POSS systems are interacting within the resins. Therefore, it is important to identify the structure and interactions occurring within the monomers, such as the degree of epoxidation and location of the Ep groups on the POSS cage. Ion mobility can detect conformers based on different sizes, so it is a vital tool in understanding the  $\text{Sty}_x\text{Ep}_{8-x}\text{T}_8$  POSS monomer structures. The ion mobility results give unique feedback to synthetic chemists on the number and location of epoxides, so that a rational synthesis of a known species can be developed.

**TOF Mass Spectrometry.** A MALDI-TOF mass spectrum of the  $\text{Sty}_x\text{Ep}_{8-x}\text{T}_8$  POSS system doped with NaI is shown in Figure 1. Only ions for  $x = 4$  to 8 are observed in the mass spectrum. Ion mobility results for  $\text{Na}^+\text{Sty}_8\text{T}_8$  have been published,<sup>34</sup> so this system will not be discussed here. The abundance of  $\text{Na}^+\text{Sty}_4\text{Ep}_4\text{T}_8$  was too small for ion mobility analysis, so only data for the analysis of  $\text{Na}^+\text{Sty}_7\text{Ep}_1\text{T}_8$ ,  $\text{Na}^+\text{Sty}_6\text{Ep}_2\text{T}_8$ , and  $\text{Na}^+\text{Sty}_5\text{Ep}_3\text{T}_8$  will be discussed. For the ion mobility experiments, the appropriate  $\text{Na}^+\text{Sty}_x\text{Ep}_{8-x}\text{T}_8$  ions are gently injected into the drift cell and their arrival time distributions (ATDs) collected. Typical ATDs are shown in Figure 2 for sodiated  $\text{Sty}_7\text{Ep}_1\text{T}_8$ ,  $\text{Sty}_6\text{Ep}_2\text{T}_8$ , and  $\text{Sty}_5\text{Ep}_3\text{T}_8$ .

**$\text{Na}^+\text{Sty}_7\text{Ep}_1\text{T}_8$ .** Three resolvable features are apparent in the  $\text{Na}^+\text{Sty}_7\text{Ep}_1\text{T}_8$  ATD, indicating that three distinct conformers with different mobilities exist. To better analyze these features, the temperature of the drift cell was decreased

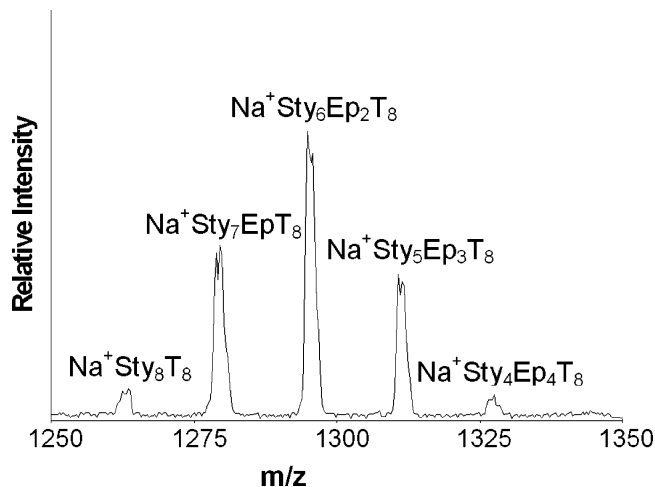


**Figure 1.** MALDI-TOF mass spectrum of the sodiated  $\text{Sty}_x\text{Ep}_{8-x}\text{T}_8$  sample.

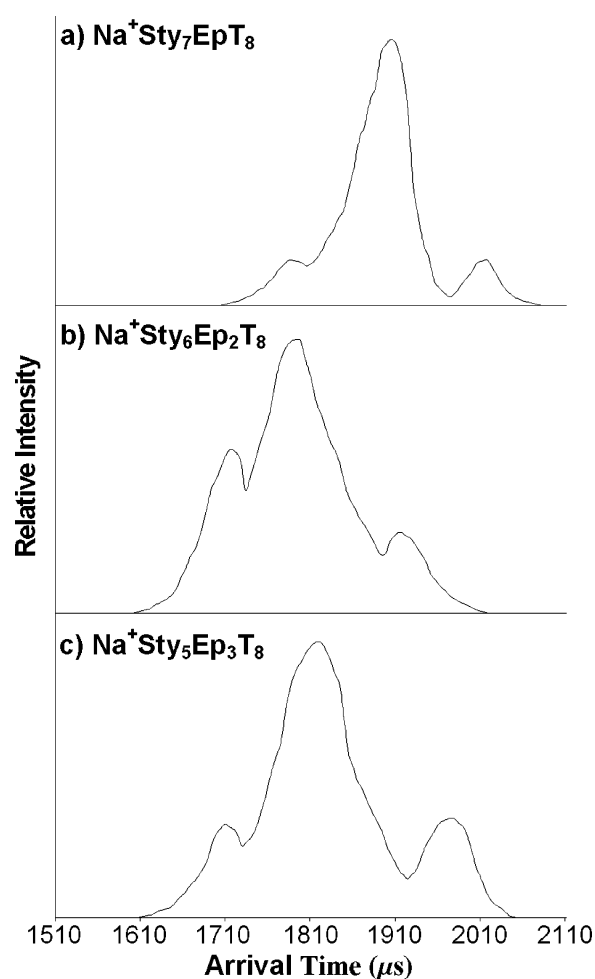


**Figure 2.** Arrival time distributions (ATDs) of (a)  $\text{Na}^+\text{Sty}_7\text{Ep}_1\text{T}_8$ , (b)  $\text{Na}^+\text{Sty}_6\text{Ep}_2\text{T}_8$ , and (c)  $\text{Na}^+\text{Sty}_5\text{Ep}_3\text{T}_8$  obtained at a drift cell temperature of 120 K for best resolution. The multiple peaks in the ATDs represent multiple conformations of the ion that have different collision cross-sections.

from 300 to 120 K to slow any possible isomerization and to increase the resolution of the ATD peaks.<sup>35–37</sup> As the temperature was lowered, no new peaks were detected but the resolution of the ATDs increased. Therefore, Figure 2 illustrates only the high-resolution ATDs at 120 K. The

**Table 1.** Collision Cross-Sections ( $\text{\AA}^2$ ) and Abundances for  $\text{Na}^+\text{Sty}_7\text{EpT}_8$ ,  $\text{Na}^+\text{Sty}_6\text{Ep}_2\text{T}_8$ , and  $\text{Na}^+\text{Sty}_5\text{Ep}_3\text{T}_8$

name	experiment	theory <sup>a</sup>	% abundance <sup>b</sup>	statistical abundance
$\text{Na}^+\text{Sty}_7\text{EpT}_8$	319	320 (a)	13%	22%
	323	324 (b)	74%	69%
	327	328 (c)	13%	9%
$\text{Na}^+\text{Sty}_6\text{Ep}_2\text{T}_8$	315	314 (d)	22%	43%
	319	319 (e)	66%	43%
	324	322 (f)	12%	14%
$\text{Na}^+\text{Sty}_5\text{Ep}_3\text{T}_8$	314	314 (g)	17%	40%
	319	319 (h)	66%	40%
	327	326 (i)	17%	20%

<sup>a</sup> Calculated average cross-sections for the (a) “three-pair” family, (b) “two-pair” family, (c) “one-pair” family, (d) two Ep on adjacent corners, (e) two Ep face-diagonal, (f) two Ep on opposite corners, (g) three Ep on adjacent corners, (h) two Ep on adjacent corners, and (i) Ep on opposite corners. <sup>b</sup> Abundances from relative intensities of ATD peaks.

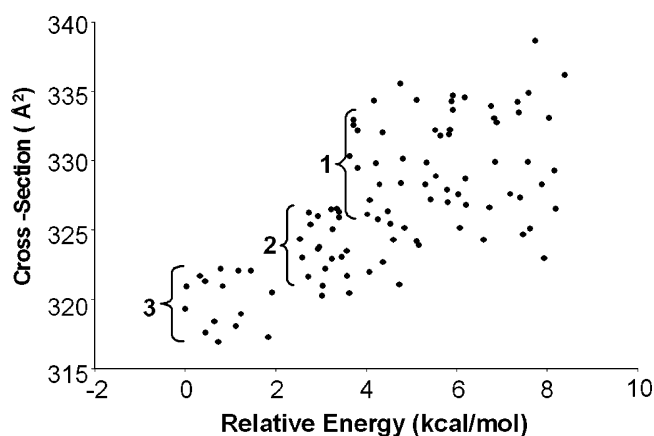


**Figure 3.** Plot of cross-section vs energy for  $\text{Na}^+\text{Sty}_7\text{EpT}_8$ . Each point represents one theoretical structure generated by the simulated annealing method. Three families of structures are predicted that differ in the number of paired Sty groups (see Figure 4).

collision cross-sections of each ATD peak are extracted at 300 K using eqs 1 and 2 (in the Supporting Information), and these values and the relative abundance of each peak are listed in Table 1. The shape of the ATD peaks did not change as a function of injection energy (300–500 eV), so the relative intensities should be accurate representations of the abundance of each conformer exiting the MALDI source.

Theoretical structures of  $\text{Na}^+\text{Sty}_7\text{EpT}_8$  are generated by placing one Ep group on a corner of the  $\text{Si}_8\text{O}_{12}$  cube and

Sty groups on the remaining seven corners. Using the methods described in the theoretical section, a simulated annealing cycle is used to produce 100 low-energy structures for  $\text{Na}^+\text{Sty}_7\text{EpT}_8$ ,  $\text{Na}^+\text{Sty}_6\text{Ep}_2\text{T}_8$ , and  $\text{Na}^+\text{Sty}_5\text{Ep}_3\text{T}_8$ . After the structures are generated, their angle-averaged collision cross-sections are calculated using a previously developed projection model described in the Supporting Information. Cross-sections and energies are then plotted for each theoretical structure to help identify the ions observed in the ATDs. The scatter plot observed for  $\text{Na}^+\text{Sty}_7\text{EpT}_8$  is illustrated in Figure 3.

The scatter plot shows three distinct families of conformers (labeled “3”, “2”, and “1” in Figure 3) that differ in energy and cross-section. Examples of each family are shown in Figure 4. In each family, the Ep and the Sty groups extend away from the Si–O cage and the  $\text{Na}^+$  ion coordinates to one oxygen on the cage and the oxygen associated with the epoxy group. The phenyl group of Ep interacts with a phenyl group of a neighboring Sty substituent in a “tilted T”<sup>38</sup> arrangement. In this arrangement, the Ep phenyl is 5  $\text{\AA}$  away from and approximately perpendicular to the Sty phenyl group (see inset in Figure 4).

The families of structures differ in how the remaining Sty groups interact with each other. Along with the Sty–Ep “pair”, two nearest-neighbor Sty groups can form pairs in which the two phenyl groups are parallel to each other (not stacked) and displaced by 5  $\text{\AA}$ . These Sty–Sty pairs are shown in blue in Figure 4. “Unpaired” Sty groups maintain a 10  $\text{\AA}$  distance between phenyl groups. No more than two phenyl groups form a given pair, and each pair does not interact with any other Sty groups. Since six Sty groups are available for pairing (there is always one Sty–Ep pair), one, two, or three Sty–Sty pairs can form. This Sty–Sty pairing was also observed in the structures of  $\text{Na}^+\text{Sty}_8\text{T}_8$ .<sup>34</sup>

In the lowest energy family of structures, all eight Sty–Ep substituents are paired. The Ep group pairs with a Sty group to form a “tilted T” pair, while the remaining six Sty groups form three Sty–Sty pairs. Consequently, this “three-pair” family has the smallest cross-section (320  $\text{\AA}^2$ ). The second family of structures, which is  $\sim 3$  kcal/mol higher in energy and 4  $\text{\AA}^2$  larger in cross-section, has two Sty–Sty pairs along with the Sty–Ep pair. The two unpaired Sty groups are nearest neighbors but remain 10  $\text{\AA}$  from each other and the other pairs. The third family of structures, which is  $\sim 4$  kcal/mol higher in energy and 8  $\text{\AA}^2$  larger in

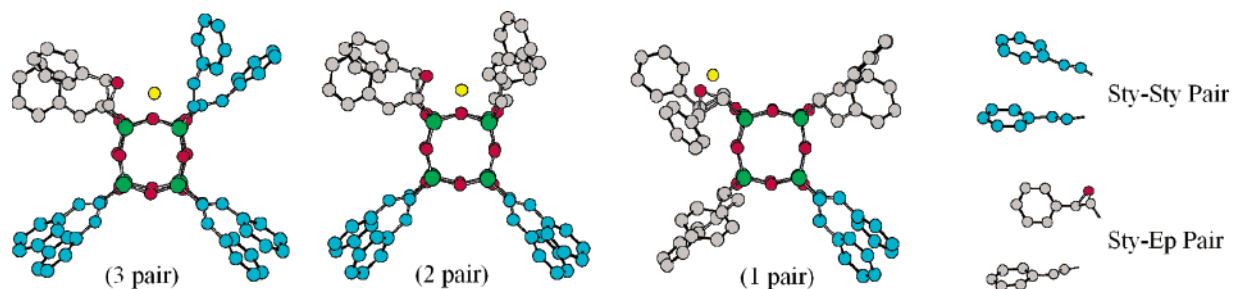


**Figure 4.** The three distinct conformers calculated for  $\text{Na}^+\text{Sty}_7\text{EpT}_8$ . Sty–Sty pairs are colored blue, carbon atoms are gray, silicon is green, oxygen atoms are red, and sodium is yellow (hydrogen atoms have been omitted for clarity). Sty–Ep “pairs” have a “tilted T” conformation, and Sty–Sty “pairs” have a “displaced parallel” conformation (shown in inset).

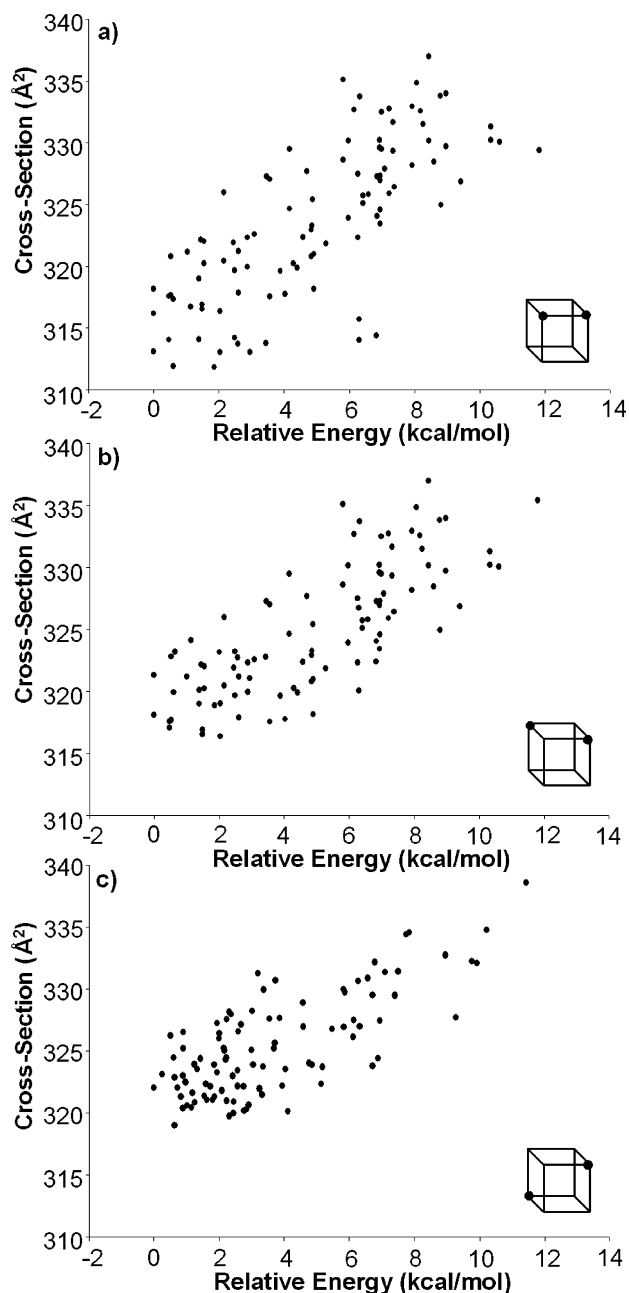


**Figure 5.** Plots of cross-section vs energy for the three geometric isomers of  $\text{Na}^+\text{Sty}_6\text{Ep}_2\text{T}_8$  with the two Ep groups (a) on adjacent corners, (b) face-diagonal to each other, and (c) on opposite corners of the Si–O cage. One low-energy family of structures is predicted for each isomer.

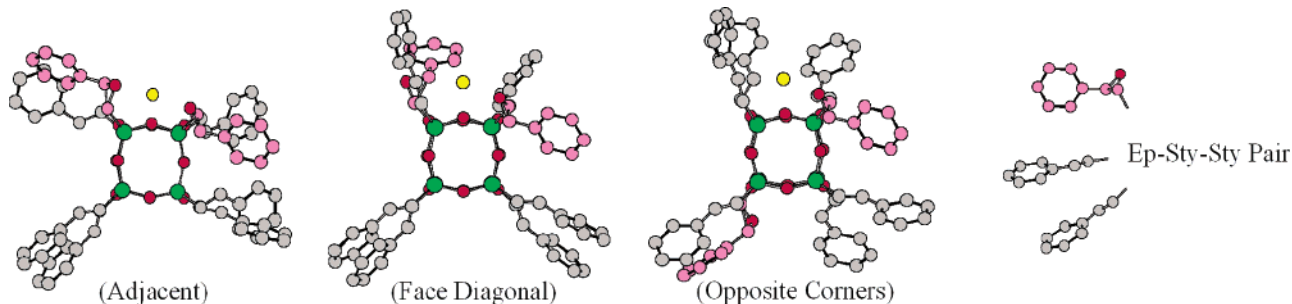


**Figure 6.** The lowest-energy structures calculated for the three isomers of  $\text{Na}^+\text{Sty}_6\text{Ep}_2\text{T}_8$ . The Ep groups are shown in pink. In the face-diagonal isomer, an Ep group couples to a Sty–Sty pair resulting in an Ep–Sty–Sty trio.

cross-section than the “three-pair” family, has one Sty–Sty pair and one Sty–Ep pair.

The calculated cross-section of each family of  $\text{Na}^+\text{Sty}_7\text{EpT}_8$  structures is compared to experimental values in Table 1. The cross-section from the shortest-time ATD peak (see Figure 2a) agrees very well with the cross-section for the “three-pair” family. The cross-section from the intermediate ATD peak, which is the most abundant peak, matches the cross-section of the family with two Sty–Sty pairs, and the cross-section from the longest-time ATD peak corresponds with that of the one Sty–Sty pair family. The observed distribution is quite similar to that predicted from a statistical placement of the Sty–Sty pairs. A similar statistical distribution was observed for Sty–Sty pairing in the  $\text{Na}^+\text{Sty}_8\text{T}_8$  system, indicating the minor energy differences predicted by AMBER for the isomers does not strongly affect the observed distribution.

**$\text{Na}^+\text{Sty}_6\text{Ep}_2\text{T}_8$ .** A typical 120 K ATD for sodiated  $\text{Sty}_6\text{Ep}_2\text{T}_8$  is shown in Figure 2b. As with  $\text{Na}^+\text{Sty}_7\text{EpT}_8$ , three resolvable features appear in the ATD for  $\text{Na}^+\text{Sty}_6\text{Ep}_2\text{T}_8$  that do not interconvert or change in intensity with injection energy. The experimental cross-section and relative abundance of each peak is listed in Table 1.

With more than one Ep group present on the  $\text{T}_8$  cage, several isomers are possible for  $\text{Sty}_6\text{Ep}_2\text{T}_8$  based on the relative positions of the Ep groups. The two Ep groups can either be placed on adjacent corners of the Si–O cage, on opposite corners on the same face of the cage, or on opposite corners of the entire cage. The scatter plots of cross-section versus energy for the 100 theoretical structures predicted for each isomer is shown in Figure 5. In each case, only one family of conformers is predicted and the lowest-energy structures displayed in Figure 6.

The isomer with the Ep groups on adjacent corners of the Si–O cage has the smallest average cross-section ( $314 \pm 4 \text{ \AA}^2$ ) of the three isomers. The  $\text{Na}^+$  ion lies between the two Ep groups and coordinates to one oxygen on the Si–O cage and the two oxygens associated with the epoxy groups. All eight of the Sty and Ep groups form “pairs”. Four of the six Sty groups form two Sty–Sty pairs and the other two Sty groups interact with the two Ep groups to form two Sty–Ep pairs. As in the  $\text{Na}^+\text{Sty}_7\text{EpT}_8$  case, only two Sty or Ep groups are involved in a given pair and none of the pairs interact with any other pair. The two Ep groups do not form an Ep–Ep pair due to the nature of the  $\text{Na}^+\text{–O}$  interactions. In order

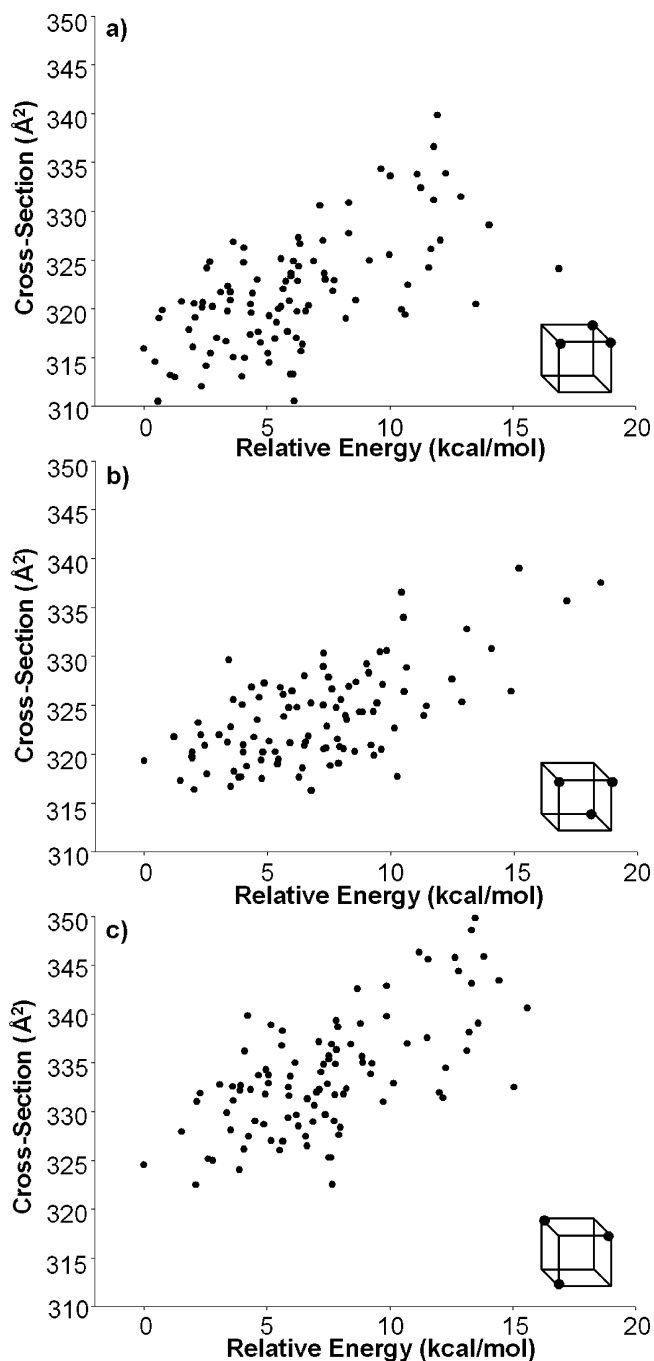


**Figure 7.** Plots of cross-section vs energy for  $\text{Na}^+\text{Sty}_5\text{Ep}_3\text{T}_8$  with (a) all three Ep groups on adjacent corners, (b) two Ep groups adjacent and the third on an opposite corner, and (c) all three Ep groups on opposite corners. One family of low-energy structures is predicted for each isomer.

for the two epoxy oxygens to be in a good position to coordinate to  $\text{Na}^+$ , the two phenyl groups must rotate away from each other, thus preventing an Ep–Ep pair from forming. However, this rotation also puts the Ep phenyl groups in a good position to form a “tilted T” pair with a neighboring Sty group.

A face-diagonal positioning of the Ep groups leads to a slightly different structure with an average cross-section ( $319 \pm 4 \text{ \AA}^2$ ) that is  $5 \text{ \AA}^2$  larger than the isomer with Ep groups on adjacent corners. In this case,  $\text{Na}^+$  lies between an Ep

and Sty group and coordinates to one oxygen on the Si–O cage, the epoxy oxygen on the Ep group, and the vinyl linkage on the Sty group (similar to the  $\text{Na}^+$  coordination in  $\text{Na}^+\text{Sty}_7\text{EpT}_8$ ). As with the “adjacent” isomer, four of the six Sty groups in the “face-diagonal” isomer form two Sty–Sty pairs. However, only one Sty–Ep pair forms (involving the Sty and Ep groups not coordinated to  $\text{Na}^+$ ). As in the “adjacent” isomer, the Sty and Ep groups coordinated to  $\text{Na}^+$  cannot form a pair because the phenyl group on Ep rotates away from the Sty group so that the epoxy oxygen can coordinate to  $\text{Na}^+$ . However, unlike the “adjacent” isomer in which the two Ep groups paired with neighboring Sty groups, the Sty group in this isomer is pulled toward the  $\text{Na}^+$  ion and cannot pair with any neighboring Sty groups. The Ep group, on the other hand, actually interacts with a Sty–Sty “pair” forming an Ep–Sty–Sty trio. This is the first example of more than two Sty or Ep groups being coordinated in a given unit.

The isomer with the Ep groups on opposite corners of the cage has the largest average cross-section ( $322 \pm 4 \text{ \AA}^2$ ) of the three isomers. As in the “face-diagonal” isomer, the  $\text{Na}^+$  ion lies between an Ep and Sty group and coordinates to one oxygen on the Si–O cage, one Ep oxygen, and a vinyl group on Sty. In this case, the two Ep groups pair with neighboring Sty groups to form two Sty–Ep pairs, but only one Sty–Sty pair is formed. The Sty group coordinated to  $\text{Na}^+$  is unpaired for the same reasons as the unpaired Sty groups in the “face-diagonal” isomer. The remaining unpaired Sty group is on the opposite corner of the Si–O cage. It appears to be simply the “odd man out” as all of its nearest neighbors are paired with other groups. However, this Sty group is in a position to form an Ep–Sty–Sty trio, similar to the one observed in the “face-diagonal” isomer, yet remains unpaired. The reason is that the Sty group is slightly pulled toward the other Ep group (not coordinated to  $\text{Na}^+$ ) and away from the Sty group necessary to form the Ep–Sty–Sty trio.

The calculated cross-section of each  $\text{Na}^+\text{Sty}_6\text{Ep}_2\text{T}_8$  isomer is compared to experimental values in Table 1. The cross-section from the shortest-time ATD peak (Figure 2b) agrees well with the theoretical value for the isomer with the Ep groups placed on adjacent corners of the Si–O cage. The cross-section from the intermediate ATD peak matches that of the “face-diagonal” isomer, and the peak at the longest time in the ATD corresponds to the isomer with Ep groups in opposite corners of the cage. The peak corresponding to the isomer with Ep groups diagonal on the face of the Si–O cage is the most abundant peak in the ATD, indicating that the “face-diagonal” isomer is the most abundant isomer produced in the synthesis. In this system only modest agreement with a pure statistical distribution of epoxy groups is obtained. Here, either energetic or steric effects (or both) are at play in the synthesis. Of importance is the fact that the three classes of epoxidation can be separated and their abundances determined.

**$\text{Na}^+\text{Sty}_5\text{Ep}_3\text{T}_8$ .** A typical 120 K ATD for  $\text{Na}^+\text{Sty}_5\text{Ep}_3\text{T}_8$  is shown in Figure 2c. Like the other two Sty–Ep compounds, the ATD for  $\text{Na}^+\text{Sty}_5\text{Ep}_3\text{T}_8$  has three peaks where

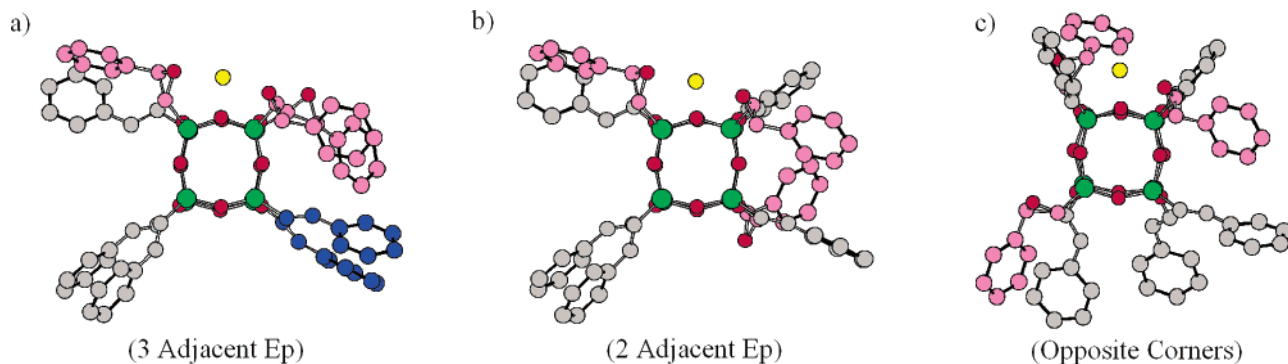


**Figure 8.** Lowest-energy structures calculated for the three isomers of  $\text{Na}^+\text{Sty}_5\text{Ep}_3\text{T}_8$ . The Ep groups are shown in pink. In the isomer with three adjacent Ep groups, two Sty–Ep pairs are paired together by a Sty–Sty interaction. The interacting Sty groups are shown in dark blue.

the middle peak is the most intense. The experimental cross-sections and relative abundances derived from the three ATD peaks at 300 K are listed in Table 1.

As with  $\text{Na}^+\text{Sty}_6\text{Ep}_2\text{T}_8$ , three isomers are possible for  $\text{Na}^+\text{Sty}_5\text{Ep}_3\text{T}_8$  depending on the positioning of the Ep groups on the Si–O cage. The three Ep groups can be placed on adjacent corners of the Si–O cage, two Ep groups can be placed on adjacent corners, and the third Ep placed on an opposite corner of the cage, or all three Ep groups can be placed on opposite corners of the cage. Plots of cross-section versus energy for the 100 generated structures of each isomer are shown in Figure 7. In each case, only one family of conformers is predicted and the lowest-energy structures for each isomer are displayed in Figure 8.

The isomer with all three Ep groups on adjacent corners of the Si–O cage (Figure 8a) has the smallest average cross-section ( $314 \pm 4 \text{ \AA}^2$ ) of the three isomers. The  $\text{Na}^+$  ion lies between two of the Ep groups and coordinates to one oxygen on the Si–O cage and the two epoxy oxygens on the Ep groups. All of the Sty and Ep groups are paired. The three Ep groups pair with neighboring Sty groups to form three Sty–Ep pairs, and the remaining two Sty groups, which are nearest neighbors, form one Sty–Sty pair. However, unlike any of the other Sty–Ep systems, two pairs interact with each other in this isomer. Two Sty groups involved in Sty–Ep pairing interact to form a Sty–Sty pair as well (shown in blue in Figure 8a), leading to a more compact structure.

The isomer with two Ep groups on adjacent corners of the Si–O cage and the third Ep on an opposite corner (Figure 8b) has an average cross-section ( $319 \pm 4 \text{ \AA}^2$ ), which is  $5 \text{ \AA}^2$  larger than the “three adjacent” isomer described above. The  $\text{Na}^+$  interactions and the Sty/Ep pairing are similar to those observed in the “three adjacent” isomer. The  $\text{Na}^+$  ion coordinates to one oxygen on the Si–O cage and two epoxy oxygens, which results in the formation of three Sty–Ep pairs and one Sty–Sty pair. The difference, and hence larger cross-section, is that none of the pairs interact with any other pairs.

The isomer with the three Ep groups on opposite corners of the Si–O cage (Figure 8c) has the largest average cross-section ( $326 \pm 4 \text{ \AA}^2$ ) of the three isomers. In this case,  $\text{Na}^+$  rests between a Sty and Ep group and coordinates to one oxygen on the Si–O cage, the epoxy oxygen on the Ep group, and the vinyl linkage on the Sty group. Only two

Sty–Ep pairs and one Sty–Sty pair are formed in this isomer. As in the “face-diagonal” isomer for  $\text{Na}^+\text{Sty}_6\text{Ep}_2\text{T}_8$ , the Sty group coordinated to  $\text{Na}^+$  is not involved in a pair because it is pulled slightly toward the  $\text{Na}^+$  ion and away from the neighboring Ep groups. Also like the “face-diagonal” isomer, the remaining unpaired Ep group (which cannot pair with the Sty group coordinated to  $\text{Na}^+$ ) interacts with the Sty–Sty pair to form an Ep–Sty–Sty trio.

Table 1 compares the calculated cross-sections for each  $\text{Na}^+\text{Sty}_5\text{Ep}_3\text{T}_8$  isomer to those determined from the ATDs (Figure 2c). The peak with the shortest time in the ATD yields a cross-section that agrees very well with the calculated value for the isomer with all three Ep groups placed on adjacent corners. The cross-section determined from the middle peak in the ATD matches the value calculated for the isomer with the two adjacent Ep groups, and the cross-section determined from the longest time peak in the ATD corresponds to the three Ep groups on opposite corners of the cage. The middle peak is the most abundant peak in the ATD, so the isomer with only two Ep groups together is likely the most abundant isomer produced in the synthesis. Similar to the  $\text{Na}^+\text{Sty}_6\text{Ep}_2\text{T}_8$  system, only modest agreement is obtained for the three  $\text{Na}^+\text{Sty}_5\text{Ep}_3\text{T}_8$  isomers with a statistical prediction of epoxy distributions indicating that steric or energetic (or both) factors contribute. However, ion mobility can separate the three isomeric forms and yield their relative abundances.

**Summary.** Three related  $\text{Na}^+\text{Sty}_x\text{Ep}_{8-x}\text{T}_8$  POSS cage systems (with  $x = 5, 6,$  and  $7$ ) have been analyzed using ion mobility experiments and MM/MD modeling. The major findings are as follows. (1) For each system ( $x = 5, 6,$  and  $7$ ), three families of isomers are found. (2) For  $x = 5$  or  $6$ , these families correspond to the different ways the Ep groups can be distributed on the POSS cage. For  $x = 7$ , the families are associated with pairing of the Sty and Ep capping groups. (3) MM/MD modeling yields three families of structures for each value of  $x$ , in agreement with experiment. The cross-sections calculated from the low energy structures in each family agree with experiment to within 1% for all 9 systems. (4) The Sty–Sty pairs have their phenyl groups parallel to each other and about  $5 \text{ \AA}$  apart. The Sty–Ep pairs have a “tilted T” structure where the planes of the phenyl groups are at a  $\sim 90^\circ$  angle. (5) The distribution of the Ep capping

agents on the POSS cage is determined for  $x = 5$  and 6. These distributions do not agree with statistical predictions indicating that steric or energetic (or both) effects are important in placing the epoxy capping agents.

**Acknowledgment.** The Air Force Office of Scientific Research under grant F49620-03-1-0046 is gratefully acknowledged.

**Supporting Information Available:** Details of the experimental procedures and theoretical modeling used for data analysis. This material is available free of charge via the Internet at <http://pubs.acs.org>.

## References

- (1) Okada, A.; Usuki, A. *Mater. Sci. Eng. C* **1995**, *3*, 109.
- (2) Gilman, J. W. *Appl. Clay Sci.* **1999**, *15*, 31.
- (3) Gilman, J. W.; Jackson, C. L.; Morgan, A. B.; Harris, R., Jr.; Manias, E.; Giannelis, E. P.; Wuthenow, M.; Hilton, D.; Phillips, S. H. *Chem. Mater.* **2000**, *12*, 1866.
- (4) Porter, D.; Metcalfe, E.; Thomas, M. J. K. *Fire Mater.* **2000**, *24*, 45.
- (5) Zanetti, M.; Lomakin, S.; Camino, G. *Macromol. Mater. Eng.* **2000**, *279*, 1.
- (6) Armes, S. P. *Polym. News* **1995**, *20*, 233.
- (7) Godovski, D. Y. *Adv. Polym. Sci.* **1995**, *119*, 79.
- (8) An entire issue of *Chemistry of Materials* is devoted to 36 short reviews and 34 articles covering all aspects of nanocomposite hybrid inorganic–organic materials. *Chem. Mater.* **2001**, *13*, 3059–3809.
- (9) Kickelbick, G. *Prog. Polym. Sci.* **2003**, *28*, 83.
- (10) Lichtenhan, J. D. *Polymeric Materials Encyclopedia*; Salamone, J. C., Ed.; CRC Press: New York, 1996; pp 7769–7778.
- (11) Schwab, J. J.; Lichtenhan, J. D. *Appl. Organomet. Chem.* **1998**, *12*, 207.
- (12) Jeon, H. G.; Mather, P. T.; Haddad, T. S. *Polym. Int.* **2000**, *49*, 453.
- (13) Waddon, A. J.; Zheng, L.; Farris, R. J.; Coughlin, E. B. *Nano Lett.* **2002**, *2*, 1149.
- (14) Haddad, T. S.; Viers, B. D.; Phillips, S. H. *J. Inorg. Organomet. Polym.* **2002**, *11*, 155.
- (15) Fu, B. X.; Gelfer, M. Y.; Hsiao, B. S.; Phillips, S.; Viers, B.; Blanski, R.; Ruth, P. *Polymer* **2003**, *44*, 1499.
- (16) Carroll, J. B.; Waddon, A. J.; Nakade, H.; Rotello, V. M. *Macromolecules* **2003**, *36*, 6289.
- (17) Leu, C.-M.; Chang, Y.-T. Wei, K.-H. *Chem. Mater.* **2003**, *15*, 3721.
- (18) Leu, C.-M.; Reddy, G. M.; Wei, K.-H.; Shu, C.-F. *Chem. Mater.* **2003**, *15*, 2261.
- (19) Lichtenhan, J. D.; Otonari, Y.; Carr, M. J. *Macromolecules* **1995**, *28*, 4355.
- (20) Haddad, T. S.; Lichtenhan, J. D. *Macromolecules* **1996**, *29*, 234.
- (21) Xu, H.; Kuo, S.-W.; Lee, J.-S.; Chang, F.-C. *Polymer* **2002**, *43*, 5117.
- (22) Xu, H.; Kuo, S.-W.; Lee, J.-S.; Chang, F.-C. *Macromolecules* **2002**, *35*, 8788.
- (23) Kim, K.-M.; Keum, D.-K.; Chujo, Y. *Macromolecules* **2003**, *36*, 867.
- (24) Wright, M. E.; Schorzman, D. A.; Feher, F. J.; Jin, R.-Z. *Chem. Mater.* **2003**, *15*, 264.
- (25) Naka, K.; Itoh, H.; Chujo, Y. *Nano Lett.* **2002**, *2*, 1183.
- (26) Feher, F. J.; Schwab, J. J.; Tellers, D. M.; Burstein, A. *Main Group Chem.* **1998**, *2*, 123.
- (27) Bowers, M. T.; Kemper, P. R.; von Helden, G.; van Koppen, P. A. M. *Science* **1993**, *260*, 1446.
- (28) Clemmer, D. E.; Jarrold, M. F. *Mass Spectrom. Rev.* **1997**, *32*, 577.
- (29) Wyttenbach, T.; Bowers, M. T.; *Top. Curr. Chem.* **2003**, *225*, 207.
- (30) Hillenkamp, F.; Karas, M.; Beavis, R. C.; Chait, B. T. *Anal. Chem.* **1991**, *63*, 1193A.
- (31) Lee, A.; Lichtenhan, J. D. *Macromolecules* **1998**, *31*, 4970.
- (32) Lee, A.; Lichtenhan, J. D.; Reinert, W. A., Sr. *Polym. Mater. Sci. Eng.* **2000**, *82*, 235.
- (33) Li, G.; Wang, L.; Ni, H.; Pittman, C. U., Jr. *J. Inorg. Organomet. Polym.* **2002**, *11*, 123.
- (34) Baker, E. S.; Gidden, J.; Fee, D. P.; Kemper, P. R.; Anderson, S. E.; Bowers, M. T. *Int. J. Mass Spectrom.* **2003**, *227*, 205.
- (35) Gidden, J.; Wyttenbach, T.; Batka, J. J.; Weis, P.; Jackson, A. T.; Scrivens, J. H.; Bowers, M. T. *J. Am. Soc. Mass Spectrom.* **1999**, *10*, 883.
- (36) Gidden, J.; Bowers, M. T. *Eur. Phys. J. D* **2002**, *20*, 409.
- (37) Gidden, J.; Bushnell, J. E.; Bowers, M. T. *J. Am. Chem. Soc.* **2001**, *123*, 5610.
- (38) Jorgensen, W. J.; Severance, D. L. *J. Am. Chem. Soc.* **1990**, *112*, 4768.

NL049957G